Thanks are due to J. I. Langford for many helpful discussions and to Dr. L. E. Alexander and Prof. A. J. C. Wilson for their interest in this project. Thanks are also due to R. E. Entler, F. J. Musil, K. Ralston, N. L. Scott, F. C. Steinbach, J. P. Wilkins and G. J. Williams for the many calculations involved.

References

ALEXANDER, L. (1948). *J. Appl. Phys.* **19**, 1068.
ALEXANDER, L. (1950). *J. Appl. Phys.* **21**, 126.
ALEXANDER, L. (1954). *J. Appl. Phys.* **25**, 155.
BEU, K. E. (1963). *X-ray diffraction methods with estimates of accuracy and precision of these methods.* G. L. Clark, ed. *The encyclopedia of X-rays and gamma rays.* p. 709. New York: Reinhold.
BEU, K. E., MUSIL, F. J. & SCOTT, D. L. (1962). *Modifications of a commercial cylindrical powder diffraction camera for precise and accurate lattice parameter measurements.* USAEC Report GAT-T-973, Goodyear Atomic Corp.
BEU, K. E., MUSIL, F. J. & WHITNEY, D. R. (1962). *Acta Cryst.* **15**, 1292.
DUMOND, J. W. M. & HOYT, A. (1930). *Phys. Rev.* **36** 1702.
EASTABROOK, J. N. (1952). *Brit. J. Appl. Phys.* **3**, 349.
LIPSON, H. & WILSON, A. J. C. (1941). *J. Sci. Instrum* **18**, 144.
PIKE, E. R. (1957). *J. Sci. Instrum* **34**, 355.
PIKE, E. R. & WILSON, A. J. C. (1959). *Brit. J. Appl. Phys.* **10**, 57.
SCHWARZSCHILD, M. M. (1928). *Phys. Rev.* **32**, 162.
SPENCER, R. C. (1931). *Phys. Rev.* **38**, 622.
STRAUMANIS, M. E. & IEVINS, A. (1940). *The precision determination of lattice constants by the asymmetric method.* Originally published in German by Julius Springer, Berlin, and translated by K. E. Beu as USAEC Report GAT-T-643, April 15, 1959.
STRAUMANIS, M. E. & WENG, C. C. (1955). *Acta Cryst.* **8**, 367.
TAYLOR, A. & SINCLAIR, H. (1945). *Proc. Phys. Soc.* **57**, 126.

Acta Cryst. (1964). **17**, 645

Precise and Accurate Lattice Parameters by Film Powder Methods. IV. Theoretical Calculation of Axial (Vertical) Divergence Profiles, Centroid Shifts, and Variances for Cylindrical Powder Diffraction Cameras

BY J. I. LANGFORD
University College, Cardiff, Wales

E. R. PIKE
Royal Radar Establishment, Malvern, Worcs., England

AND K. E. BEU,
Goodyear Atomic Corporation, Piketon, Ohio, U.S.A.*

(*Received* 11 *June* 1963)

An analytic method, based on an expansion of Eastabrook (1952) to the first power in the deviation from the Bragg angle, is used to derive the axial-divergence line profiles, centroid shifts and variances for cylindrical powder cameras. Numerical values and profiles are given for the modified 5·76 cm Philips camera and input collimator described by Beu, Musil & Scott (1962). The profiles are compared with those obtained by Beu, Landstrom, Whitney & Pike (1964) (preceding paper) who used a graphical method, based on exact equations, for the same calculation.

Excellent agreement is found over all but the extreme ends of the angular range, $\sim 2\theta$ greater than 175° and less than 10°. At these extreme angles the graphical method is expected to give superior results, since the expansions used in the analytical approach become more slowly convergent. It is shown, however, that at the high-angle end the differences are too small to be of practical account, although at low Bragg angles the differences might be measurable.

The displacement of the centroid is found to be $-0{\cdot}025°(2\theta)$ at $10°(2\theta)$ falling to zero at about 130°, and is 0·005° at 170°. The corresponding root-mean-square breadths at these angles are, respectively, $0{\cdot}030°(2\theta)$, a minimum of about 0·002° and 0·006°.

1. Introduction

A short review of previous work on axial-divergence effects has been given by Beu, Landstrom, Whitney & Pike (1964) (preceding paper) with the conclusion that no quantitative methods for the evaluation of these effects in film powder cameras were previously available. This was remedied by a graphical calculation of line profiles based on the exact geometrical relationship between primary and diffracted rays given

* Under Contract AT-(33-2)-1 with the U.S. Atomic Energy Commission.

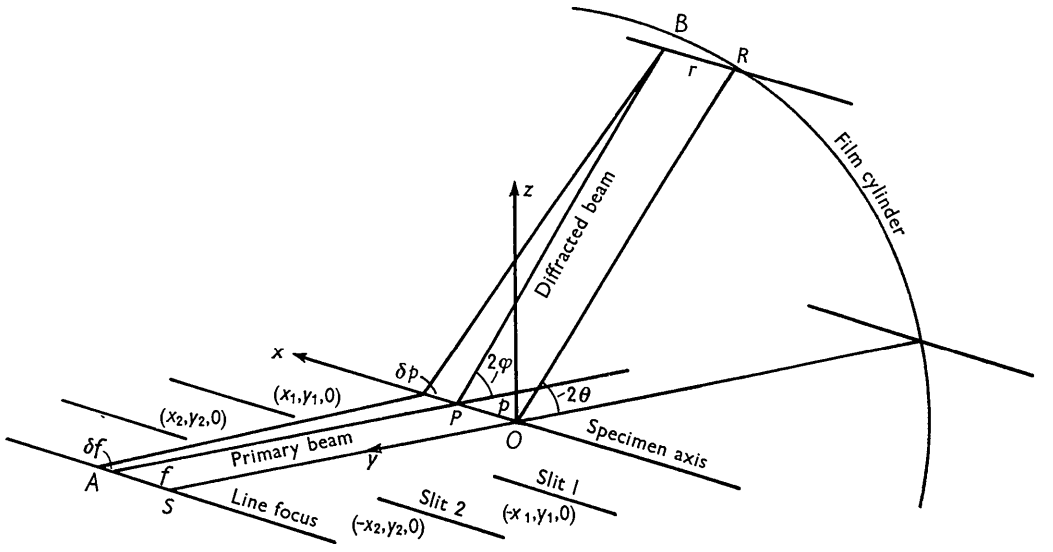

Fig. 1. Cylindrical powder camera: schematic representation of axial divergence.

by Eastabrook (1952). The method involved an intermediate machine calculation of the deviations from the Bragg angle, using this equation. Since, however, these deviations are almost always small, an alternative method is to expand the exact equation in powers of this deviation and neglect square and higher-order terms. A closed form for the deviations, first given by Eastabrook (1952, equation 12), which is valid at all but extreme Bragg angles, can be obtained in this way.

This alternative method is used in the present paper, and permits analytical expressions to be obtained for the line profile itself which are exact to the first power in the deviations. These expressions are developed in section 2.1, and results are evaluated for the same camera and collimator as were used for illustration in the previous paper. The results are compared directly.

In section 2.2 the displacement of the centroid of the line profile is calculated; our approach again allows a closed form to be derived. The method is extended to a discussion of the profile variance in section 2.3.

2. Theoretical treatment

2.1. *Line profile*

In general, axial divergence of the primary and diffracted X-ray beams causes the measured angle, 2φ, to differ from the Bragg angle, 2θ, by a small amount 2ε, such that

$$2\theta = 2\varphi + 2\varepsilon \,. \tag{1}$$

Rays from an element δf at f on the line focus (A in Fig. 1) are diffracted by an element δp at p on the specimen (P) to B on a generator of the film cylinder. If the focus is assumed to be uniform, with unit intensity per unit length, the element of intensity detected at B is

$$I(2\varepsilon)\delta(2\varepsilon) = \delta f \delta p$$

or

$$I(2\varepsilon)_p = \left[\frac{\partial f}{\partial(2\varepsilon)}\right]_p \delta p \,. \tag{2}$$

The total intensity at B, the sum of all such contributions, is

$$I(2\varepsilon) = \Sigma \left[\frac{\partial f}{\partial(2\varepsilon)}\right]_p \delta p$$

or

$$I(2\varepsilon) = \int_p \left[\frac{\partial f}{\partial(2\varepsilon)}\right] dp \,. \tag{3}$$

Eastabrook (1952) has derived an expression for 2ε. In the above notation

$$\cos(2\varphi - 2\varepsilon) = \left[\frac{(p-f)^2+S^2}{S^2}\right]^{\frac{1}{2}}\left[\frac{(r-p)^2+R^2}{R^2}\right]^{\frac{1}{2}} \cos 2\varphi - \frac{(p-f)}{S}\frac{(r-p)}{R},$$

where r is the distance of B from the equatorial plane along a generator of the film cylinder, R is the camera radius, and S is the distance between the focus and axis of rotation. Except at low and very high angles, for typical camera dimensions, this approximates to (Eastabrook, 1952, equation 12)

$$2\varepsilon = \tfrac{1}{2}\left[\frac{(p-f)^2}{S^2}+\frac{(r-p)^2}{R^2}\right]\cot 2\varphi - \frac{(p-f)}{S}\frac{(r-p)}{R}\operatorname{cosec} 2\varphi \,, \tag{4}$$

the error in 2ε being

$$\Delta(2\varepsilon) \simeq \tfrac{1}{2}(2\varepsilon)^2 \cot 2\varphi - \tfrac{1}{8}\left[\frac{(p-f)^2}{S^2} - \frac{(r-p)^2}{R^2}\right]^2 \cot 2\varphi .$$

If $S/R=\mu$,

$$(2S^2 \tan 2\varphi)(2\varepsilon) = [(p-f)^2+\mu^2(r-p)^2] - 2\mu(p-f)(r-p)\sec 2\varphi . \quad (5)$$

Re-arranging equation (5) and solving for f gives

$$f = p - \mu(r-p)\sec 2\varphi \pm \sqrt{(\mu^2(r-p)^2 \tan^2 2\varphi + (2S^2 \tan 2\varphi)(2\varepsilon))} , \quad (6)$$

and

$$\left|\frac{\partial f}{\partial(2\varepsilon)}\right|_p = \pm \frac{RS}{\sqrt{((r-p)^2+(2R^2 \cot 2\varphi)(2\varepsilon))}} . \quad (7)$$

(The positive and negative signs correspond to contributions from each side of the median plane. Since these are symmetrical, the modulus may be taken.) From equation (3),

$$I(2\varepsilon) = RS\int_p \frac{dp}{\sqrt{((r-p)^2+(2R^2 \cot 2\varphi)(2\varepsilon))}} ,$$

and the line profile is

$$\left.\begin{aligned} I(2\varepsilon) &= RS\left[\sinh^{-1}\frac{(p-r)}{\sqrt{((2R^2 \cot 2\varphi)(2\varepsilon))}}\right]_p \\ &\qquad 2\varepsilon \geq 0,\ 2\varphi < \pi/2 \\ &\qquad 2\varepsilon \leq 0,\ 2\varphi > \pi/2 \\ I(2\varepsilon) &= RS\,[\log|p-r|]_p \\ &\qquad 2\varepsilon_{\max} \geq 2\varepsilon \geq 2\varepsilon_{\min},\ 2\varphi = \pi/2 \\ I(2\varepsilon) &= RS\left[\cosh^{-1}\frac{(p-r)}{\sqrt{(2R^2\,|2\varepsilon \cot 2\varphi|)}}\right]_p \\ &\qquad 2\varepsilon \leq 0,\ 2\varphi < \pi/2 \\ &\qquad 2\varepsilon \geq 0,\ 2\varphi > \pi/2 . \end{aligned}\right\} \quad (8)$$

The limits of p in equation (8) depend upon the input collimation (we assume that the incident beam fills the collimation system). They are determined by reference to a diagram of the type illustrated in Fig. 2, in which accessible values of p and f for given ranges of 2ε are enclosed by boundary lines. These boundary lines, for slits at $(\pm x_1, y_1)$ and $(\pm x_2, y_2)$ as in Fig. 1, are given by the equations (see also Beu, Landstrom, Whitney & Pike, 1964)

$$y_1 f + (S-y_1)p \pm x_1 S = 0 \quad (9)$$

$$y_2 f + (S-y_2)p \pm x_2 S = 0 \quad (10)$$

or

$$p = -m_2 f - c_2 \quad (VM) \quad (11)$$

$$p = -m_1 f + c_1 \quad (MN) \quad (12)$$

$$p = -m_2 f + c_2 \quad (NU) \quad (13)$$

and

$$p = -m_1 f - c_1 \quad (UV) , \quad (14)$$

where

$$m_1 = \frac{y_1}{S-y_1},\ c_1 = \frac{x_1 S}{S-y_1},\ m_2 = \frac{y_2}{S-y_2} \text{ and } c_2 = \frac{x_2 S}{S-y_2} .$$

It may be shown that the 2ε contours in the (f, p) plane have a centre of symmetry at $f=p=r$. For profiles along the equatorial plane of the film cylinder ($r=0$), the centre is at the origin, and the integration may be simplified by taking $f=0$ (or $p=0$) as a boundary. For off-axis profiles, however, the entire region $VMNU$ must be taken.

The 2ε contours vary considerably for different values of 2φ and general expressions for the limits in equation (8) would be cumbersome. The general procedure for determining the limits will become apparent if the particular case of an equatorial profile at $2\varphi = 45°\ (2\theta)$ is considered. For non-equatorial profiles or other values of 2φ a similar argument applies. The 2ε curves for this case, calculated for a Philips 5·76 cm powder camera, are given in Fig. 2, and if

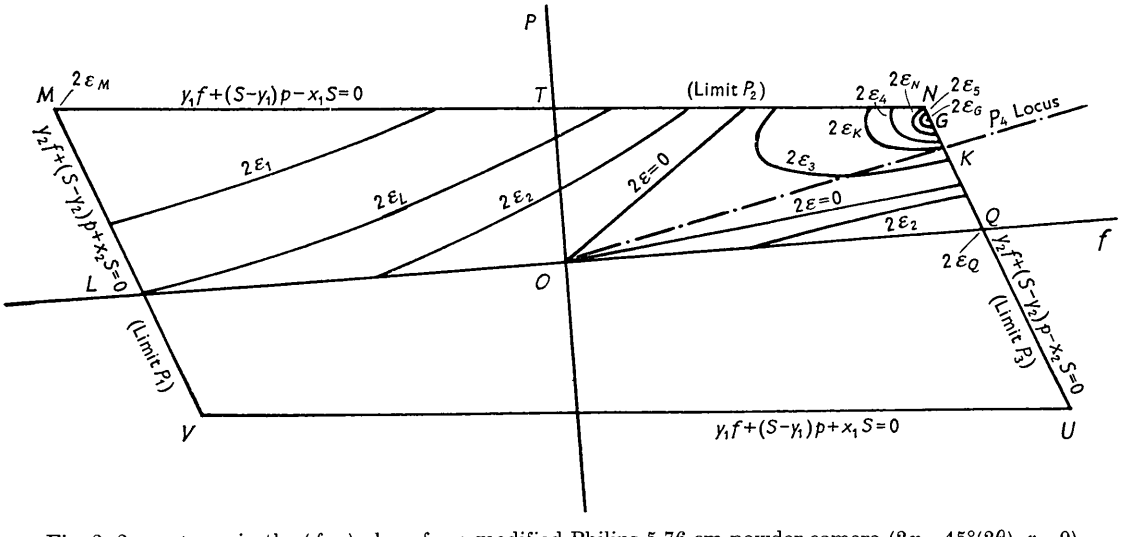

Fig. 2. 2ε contours in the (f, p) plane for a modified Philips 5·76 cm powder camera ($2\varphi = 45°(2\theta)$, $r=0$).

$$\Psi(2\varphi, 2\varepsilon, p) = \frac{(p-r)}{\sqrt{(2R^2|2\varepsilon \cot 2\varphi|)}}, \qquad (15)$$

the line profile is

$$\left.\begin{aligned}
&I(2\varepsilon) \propto [\sinh^{-1}\Psi]_{p_1}^{p_2} && 2\varepsilon_M \geq 2\varepsilon_1 \geq 2\varepsilon_L \\
&I(2\varepsilon) \propto [\sinh^{-1}\Psi]_{0}^{p_2} + [\sinh^{-1}\Psi]_{0}^{p_3} && \\
& && 2\varepsilon_L \geq 2\varepsilon_2 > 0 \\
&I(2\varepsilon) = \infty && 2\varepsilon = 0 \\
&I(2\varepsilon) \propto [\cosh^{-1}\Psi]_{p_4}^{p_2} + [\cosh^{-1}\Psi]_{p_4}^{p_3} && \\
& && 0 > 2\varepsilon_3 \geq 2\varepsilon_K \\
&I(2\varepsilon) \propto [\cosh^{-1}\Psi]_{p_3}^{p_2} && 2\varepsilon_K \geq 2\varepsilon_4 \geq 2\varepsilon_N \\
&I(2\varepsilon) \propto [\cosh^{-1}\Psi]_{p_3}^{p_3} && 2\varepsilon_N \geq 2\varepsilon_5 \geq 2\varepsilon_G
\end{aligned}\right\} \qquad (16)$$

where p_1 satisfies equations (6) and (11), p_2 satisfies equations (6) and (12), p_3 satisfies equations (6) and (13). p_4 is the minimum value of p for each 2ε and it divides those 2ε curves which are double-valued into two single-valued sections which can then be used to calculate $I(2\varepsilon)$ in the range of $0 > 2\varepsilon_3 > 2\varepsilon_K$. This occurs when $2\varepsilon \cot 2\varphi < 0$, and the second term of equation (6) is zero. (It is also the value for which $\cosh^{-1}\Psi \equiv 0$, and thus need not be evaluated.) The locus of p_4 is given by

$$f = p - \mu(r-p)\sec 2\varphi\,. \qquad (17)$$

The zones of 2ε over which equations (16) are applicable are determined at each 2φ (and different r) as follows.

(*a*) $2\varepsilon = 0$

From equation (6), the region bounded by $2\varepsilon = 0$ lies between the two straight lines

$$f = p - \mu(r-p)(\sec 2\varphi \mp \tan 2\varphi)\,, \qquad (18)$$

and the lines intersect at $f = p = r$.

(*b*) $2\varepsilon = 2\varepsilon_M (2\varepsilon_{\max}$ for $2\varphi < \pi/2)$

$2\varepsilon_M$ is given by the substitution of (f_M, p_M) in equation (4).

(*c*) $2\varepsilon = 2\varepsilon_N (2\varepsilon_{\min}$ for $2\varphi > \pi/2)$

$2\varepsilon_N$ is given by the substitution of (f_N, p_N) in equation (4).

(*d*) $2\varepsilon = 2\varepsilon_L$ $(= 2\varepsilon_Q$ for $r = 0)$

$2\varepsilon_L[2\varepsilon_Q]$ is given by the substitution of $(f_L, 0)$ $[(f_Q, 0)]$ in equation (4).

(*e*) $2\varepsilon = 2\varepsilon_K$

$2\varepsilon_K$ is the value of 2ε corresponding to the intersection of the locus of p_4 and one of the boundaries. (LM, MN, NQ for $r = 0$, VM, MN, NU, UV for $r \neq 0$.)

(*f*) $2\varepsilon = 2\varepsilon_G$ ($2\varepsilon_{\min}$ for $2\varphi < \pi/2$; $2\varepsilon_{\max}$ for $2\varphi > \pi/2$.)

This is obtained by solving equation (6) with (11), (12) or (13) (or 14 when $r \neq 0$) for p and differentiating with respect to 2ε.

The example chosen involves all possible 2ε zones. At other angles there may be no contribution from some zones and in many cases the contribution to the intensity will be negligibly small.

There are thus three stages in the determination of the line-profile arising from axial divergence at a particular 2φ or r.

1. The zones of the 2ε contours in the (f, p) plane are determined.
2. The p limits corresponding to each 2ε curve are calculated.
3. The intensities at each 2ε are computed.

These operations may all be performed on a computer and, to give an indication of the magnitude of the effect of axial divergence on the diffracted inten-

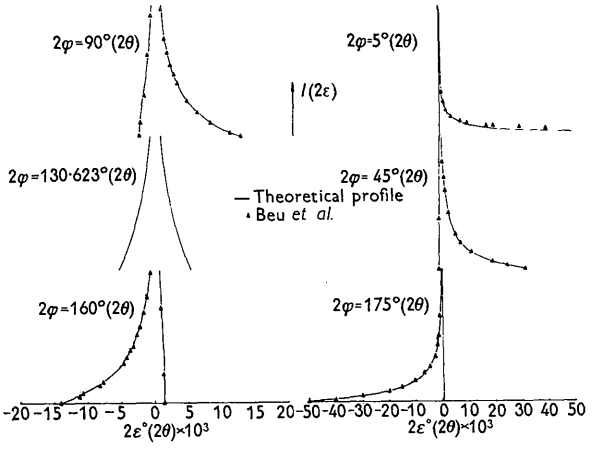

Fig. 3. Intensity profiles for a modified Philips 5·76 cm powder camera ($r = 0$).

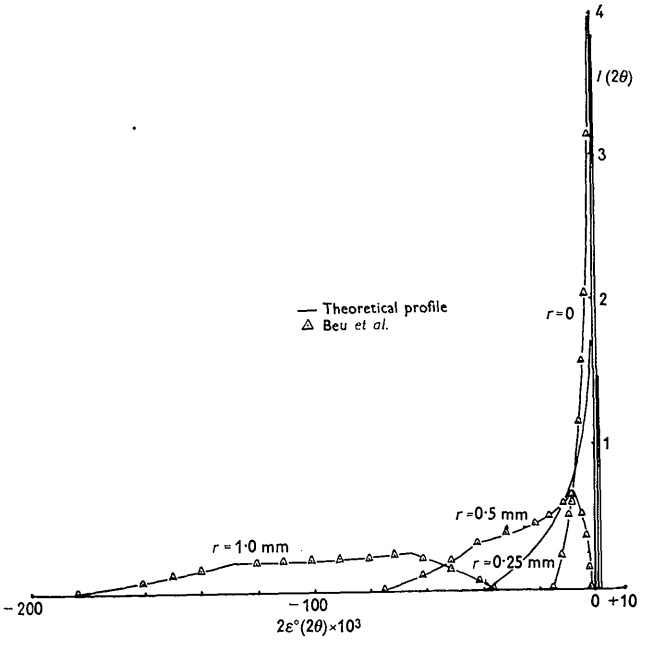

Fig. 4. Intensity profiles for a modified Philips 5·76 cm powder camera (Non-equatorial profiles, $2\varphi = 160°$ (2θ)).

sity, a Stantec ZEBRA has been used to compute the profiles at various angles for a modified Philips 5·76 cm camera (Beu, Musil & Scott, 1962). For this camera, $S=9{\cdot}55$ cm, $x_1=0{\cdot}25$ mm, $y_1=6{\cdot}8$ mm, $x_2=0{\cdot}50$ mm and $y_2=49{\cdot}8$ mm. The axial divergence profiles for the equatorial case ($r=0$) at various 2φ are given in Fig. 3 and for various r, $2\varphi=160°$ (2θ) in Fig. 4. Intensities calculated by the graphical method described in the preceding paper for the same experimental conditions are also given in Figs. 3 and 4.

2.2. *Centroid displacement*

Axial divergence displaces the centroid of the profile by

$$\langle 2\varepsilon\rangle = \frac{\iiint 2\varepsilon(f,p,r)dp\,df\,dr}{\iiint dp\,df\,dr}. \tag{19}$$

While equation (19) may be evaluated for any value of r, only the simple case of $r=0$ will be considered (corresponding to a detector whose 'window' dimensions are small). The integration is then over the region $LMNQ$ (Fig. 2) and the limits are defined by equations (11)–(13) and $p=0$. The integration is further simplified if the f,p axes are rotated through angles ζ, $-\xi$ to f', p' where

$$\tan\zeta = m_1 \tag{20}$$

and

$$\tan\xi = m_2\,. \tag{21}$$

Then

$$\begin{pmatrix} f \\ p \end{pmatrix} = \begin{pmatrix} \cos\zeta & -\sin\xi \\ -\sin\zeta & \cos\xi \end{pmatrix} \begin{pmatrix} f' \\ p' \end{pmatrix} \tag{22}$$

and

$$\langle 2\varepsilon\rangle = \frac{\iint 2\varepsilon(f',p')\dfrac{\partial(f',p')}{\partial(f,p)}dp'\,df'}{\iint \dfrac{\partial(f',p')}{\partial(f,p)}dp'\,df'}. \tag{23}$$

From equation (22),

$$\begin{pmatrix} f' \\ p' \end{pmatrix} = \frac{1}{\cos(\zeta+\xi)} \begin{pmatrix} \cos\xi & \sin\xi \\ \sin\zeta & \cos\zeta \end{pmatrix} \begin{pmatrix} f \\ p \end{pmatrix}, \tag{24}$$

giving

$$\frac{\partial(f',p')}{\partial(f,p)} = \frac{1}{\cos(\zeta+\xi)}. \tag{25}$$

The centroid displacement ($r=0$) is thus

$$\langle 2\varepsilon\rangle = \frac{\iint 2\varepsilon(f',p')dp'df'}{\iint dp'df'}, \tag{26}$$

where the limits of integration are

$$f'_L \le f' \le f'_Q \text{ (or } -F' \le f' \le F'),$$
$$0 \le p' \le p'_T \text{ (or } 0 \le p' \le P').$$

Referred to axes (f', p'), with $r=0$, equation (5) becomes

$$2\varepsilon(f',p') = A(f')^2 + Bf'p' + C(p')^2 \tag{27}$$

where ζ, ξ are given by equations (20) and (21),

$$\left.\begin{aligned} A &= (1/S^2)[1+(1+\mu\sec 2\varphi)\sin 2\zeta \\ &\qquad +\mu(\mu+2\sec 2\varphi)\sin^2\zeta)] \\ B &= -(2/S^2)[\sin(\zeta+\xi)+(1+\mu\sec 2\varphi)\cos(\zeta-\xi) \\ &\qquad +\mu(\mu+2\sec 2\varphi)\sin\zeta\cos\xi] \\ C &= (1/S^2)[1+(1+\mu\sec 2\varphi)\sin 2\xi \\ &\qquad +\mu(\mu+2\sec 2\varphi)\cos^2\xi]\,. \end{aligned}\right\} \tag{28}$$

From equation (26),

$$\langle 2\varepsilon\rangle = \frac{\int_{-F'}^{F'}\int_0^{P'}[A(f')^2+Bf'p'+C(p')^2]dp'\,df'}{\int_{-P'}^{F'}\int_0^{P'}dp'df'},$$

or

$$\langle 2\varepsilon\rangle = \tfrac{1}{3}[A(F')^2+C(P')^2]\,. \tag{29}$$

F' is given by the transform of equation (13),

$$-\sin\zeta F' = -m_2\cos\zeta F' + c_2$$

or

$$F' = c_2\sqrt{(1+m_1^2)}/(m_2-m_1)\,, \tag{30}$$

and P' is given by the transform of equation (12),

$$\cos\xi P' = m_1\sin\xi + c_1$$

or

$$P' = c_1\sqrt{(1+m_2^2)}/(m_2-m_1)\,. \tag{31}$$

Substituting for F', P' in equation (29),

$$\begin{aligned} \langle 2\varepsilon\rangle &= \frac{1}{6S^2(m_2-m_1)^2} \\ &\times[c_2^2\{[(1+m_1)^2+\mu_2 m_1^2]\cot 2\varphi + 2\mu m_1(1+m_1)\operatorname{cosec}2\varphi\} \\ &+c_1^2\{[(1+m_2)^2+\mu_2 m_2^2]\cot 2\varphi + 2\mu m_2(1+m_2)\operatorname{cosec}2\varphi\}], \end{aligned} \tag{32}$$

or

$$\langle 2\varepsilon\rangle = \frac{1}{6(q_1-q_2)^2}(\alpha_2^2 Q_{11}+\alpha_1^2 Q_{22}) \tag{33}$$

where

$$2\alpha_i = \text{slit height/focus-to-slit distance}\left(=\frac{2x_i}{S-y_i}\right),$$

$$q_i = \text{specimen-to-slit distance/slit-to-focus distance}\left(=\frac{y_i}{S-y_i}\right) \tag{34}$$

and

$$\begin{aligned} Q_{ij} &= [1-q_i(\mu-1)][1-q_j(\mu-1)]\cot 2\varphi \\ &\qquad +\mu[q_i(1+q_j)+q_j(1+q_i)]\cot\varphi\,. \end{aligned}$$

For the particular case of the modified Philips 5·76 cm camera referred to in § 2.1, the centroid displacement is

$$\langle 2\varepsilon\rangle = 0{\cdot}925\cot 2\varphi + 1{\cdot}726\cot\varphi \quad °(2\theta)\times 10^3\,. \tag{35}$$

2.3. *Variance*

The variance, or mean-square broadening, of the profile is

$$W=\langle(2\varepsilon)^2\rangle-\langle 2\varepsilon\rangle^2\,, \tag{36}$$

where $\langle 2\varepsilon\rangle^2$ is obtained from equation (33) and

$$\begin{aligned}\langle(2\varepsilon)^2\rangle &= \frac{\int_{-F'}^{F'}\int_0^{P'}[2\varepsilon(f',p')]^2\,dp'\,df'}{\int_{-F'}^{F'}\int_0^{P'}dp'\,df'} \\ &= \frac{\int_{-F'}^{F'}\int_0^{P'}[A(f')^2+Bf'p'+C(p')^2]^2\,dp'\,df'}{\int_{-F'}^{F'}\int_0^{P'}dp'\,df'} \\ &= \tfrac{1}{5}A^2(F')^4+\tfrac{1}{9}(2AC+B^2)(F')^2(P')^2+\tfrac{1}{5}C^2(P')^4\,.\end{aligned} \tag{37}$$

The variance then reduces to

$$W=\frac{1}{2(q_1-q_2)^4}\{\tfrac{1}{10}\alpha_2^4Q_{11}^2+\tfrac{1}{9}\alpha_1^2\alpha_2^2(Q_{11}Q_{22}+2Q_{12}^2)+\tfrac{1}{10}\alpha_1^4Q_{22}^2\}-\langle 2\varepsilon\rangle^2\,. \tag{38}$$

For the modified Philips 5·76 cm camera the variance is

$$W=0{\cdot}995\,\cot^2 2\varphi+2{\cdot}608\,\cot 2\varphi\,\cot\varphi+7{\cdot}733\,\cot^2\varphi \quad [^\circ(2\theta)]^2\times 10^6\,. \tag{39}$$

3. Conclusions

The intensity profiles arising from axial divergence have been derived analytically, using a method based on Eastabrook's approximation of neglecting the second and higher orders of 2ε, the difference in angle between an element of the diffracted beam and the equivalent beam diffracted according to the Bragg equation. (It should be noted that 2ε is *added* to the measured angle 2φ to obtain the Bragg angle.) A general expression for the line profile would be unwieldy, but for a camera of known geometry, the procedure for obtaining it is quite straightforward. The profiles at various angles have been computed for a modified Philips 5·76 cm camera (Beu, Musil & Scott 1962).

In Fig. 3, the intensity variation along the equatorial line of the film cylinder ($r=0$) is given corresponding to that received by a detector whose 'window' dimensions are small. In all cases there is an infinity at $2\varepsilon=0$ and, except at one particular angle (determined by the collimator geometry), the profiles are asymmetric. In Fig. 4, off-axis profiles are illustrated for $2\varphi=160\,^\circ(2\theta)$. As $|r|$ departs from zero, the infinity at $2\varepsilon=0$ persists until $|r|$ attains a particular value $|r|_{\rm lim}$, and for further increases in $|r|$, the maximum intensity falls off rapidly. [$|r|_{\rm lim}$ is the value of r for which the $2\varepsilon=0$ contours just touch a boundary of the (f, p) plane.]

If the above profiles are compared with those calculated for the same camera by the graphical method of Beu, Landstrom, Whitney & Pike (1964), it will be seen that there is negligible discrepancy between the results of the two methods except at low and very high angles. Though the differences are unlikely to be significant in practice, the graphical procedure should give a better approximation to the exact intensity in these regions. At intermediate angles, the use of an analytical method obviates the difficulties arising from the infinity at $2\varepsilon=0$.

The expressions for the centroid displacement and mean-square broadening (the variance) are quite general and again give a sufficiently good approximation in practice except at low or very high angles. The centroid displacement, given by equation (33), is zero at the angle for which the line profile is symmetrical, positive for lower angles and negative at higher angles. The variance, given by equation (38), passes through a minimum at the same angle. For the above camera, the shift in centroid, from equation (35), is given in Fig. 5, and the variance, from equation 39, is given in Fig. 6, for various 2φ. The centroid displacement is $-0{\cdot}025^\circ$ at 10° (2θ), falling to zero at about 130° (2θ) and is $+0{\cdot}005^\circ$ at 170° (2θ). The corresponding root-mean-square breadths at these angles are, respectively, $0{\cdot}030^\circ$, a minimum of about $0{\cdot}002^\circ$ and $0{\cdot}006^\circ$. Thus the centroid displacement and breadth due to axial divergence for this particular camera geometry are comparatively small, except at low or

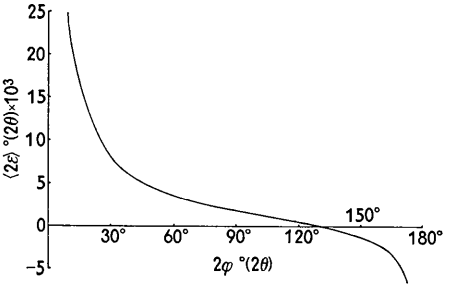

Fig. 5. Centroid displacement for a modified Philips 5·76 cm powder camera ($r=0$).

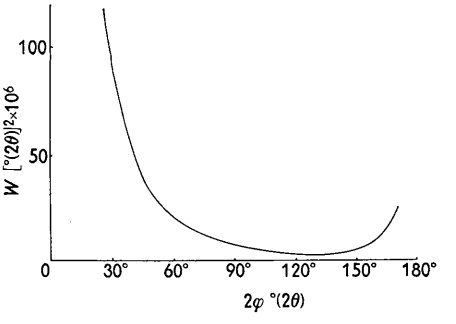

Fig. 6. Mean-square-broadening (variance) for a modified Philips 5·76 cm powder camera ($r=0$).

very high angles, and only become significant if the film is photometered to this order of accuracy. These quantities may be compared with the centroid displacement and variance which have been determined previously (Pike, 1957, 1959; Langford, 1962) for a diffractometer with various collimator geometries.

Unlike most geometrical effects, the error arising from axial divergence does not extrapolate to zero at $2\theta = 180°$. In the accurate determination of lattice parameters, therefore, it is necessary to evaluate the contribution to each diffraction maximum. If the centroid and variance are used as measures of position and breadth, the axial-divergence error is directly additive to errors from other aberrations (Pike,1957; Parish & Wilson, 1959).

We are indebted to Prof. A. J. C. Wilson for his interest in the paper and for valuable advice and criticism.

References

Beu, K. E., Landstrom, K. D., Whitney, D. R. & Pike, E. R. (1964). *Acta Cryst.* **17**, 639.
Beu, K. E., Musil, F. J. & Scott, D. L. (1962). U.S.A.E.C. Report GAT–T–973, Goodyear Atomic Corporation.
Eastabrook, J. N. (1952). *Brit. J. Appl. Phys.* **3**, 349.
Langford, J. I. (1962). *J. Sci. Instrum.* **39**, 515.
Parrish, W. & Wilson, A. J. C. (1959). In *International Tables for X-ray Crystallography*, Vol. II. Birmingham: The Kynoch Press.
Pike, E. R. (1957). *J. Sci. Instrum.* **34**, 355
Pike, E. R. (1959). *J. Sci. Instrum.* **36**, 52.

Acta Cryst. (1964). **17**, 651

Neutron Diffraction Investigation of U_3O_8*

By B. O. Loopstra

Reactor Centrum Nederland, Petten(NH), The Netherlands

(*Received* 24 *June* 1963)

A polycrystalline sample of orthorhombic U_3O_8 has been investigated by neutron diffraction in order to resolve discrepancies between previous single-crystal X-ray and powder neutron investigations. The space group is $Amm2$ (C_{2v}^{14}). The uranium atoms are surrounded by six oxygen atoms in close contact at distances between 2·07 and 2·23 Å, with a seventh oxygen atom at 2·44 Å for the U(1) atom and at 2·71 Å for the U(2) atom.

Introduction

The structure of the orthorhombic form of U_3O_8, first proposed by Zachariasen (1945), has been redetermined independently by an X-ray investigation on single crystals (Chodura & Malý, 1958) and by a neutron-diffraction investigation on powdered material (Andresen, 1958). The results from the two methods differ in many details, although the overall features are quite similar (Fig. 2). Because the investigation of Andresen made use of a neutron diagram with a rather poor resolution, it seemed worth while to repeat it, using an improved resolution, in order to get a set of experimental data more sensitive to the details of the structure.

Experimental

A high purity sample of U_3O_8 powder was mounted on the powder diffractometer at the Petten HFR. The sample was contained in a cylindrical aluminum sample holder of 0·05 mm wall thickness and 24 mm diameter. Monochromatic radiation with a wavelength of 1·092 Å was obtained from a copper (200) plane. Soller slits of 10′ angular divergence were mounted in front of the BF_3 detector and between the reactor and the monochromator. The experimental data of Table 1 were obtained in about one week with the reactor operating at 20 MW. The intensities were brought to an absolute scale by scaling from a nickel powder diagram, obtained under identical conditions. The diagram is reproduced in Fig. 1.

Results and discussion

From an X-ray diagram the unit-cell dimensions of the sample were found to be $a = 4{\cdot}14_8$, $b = 11{\cdot}96_6$ and $c = 6{\cdot}71_7$ Å. The axes have been chosen in accordance with the usual designation of the space group, derived below. To avoid confusion, all space groups mentioned have been referred to these axes.

The unit cell is in accordance with Andresen's data, whereas Chodura & Malý report an a axis of double length derived from weak layer lines on rotation

* Work sponsored jointly by Reactor Centrum Nederland, the Netherlands and Institutt for Atomenergi, Norway.

† Actually there is one weak intensity at 25·3° 2θ that cannot be indexed on the present cell. Nor, however, does it fit with an a axis of double length. It has been neglected.